Coulomb interaction effects in graphene bilayers: electron–hole pairing and plasmaron formation

2012 New J. Phys. 14 075007

(http://iopscience.iop.org/1367-2630/14/7/075007)

New Journal of Physics
The open-access journal for physics

Coulomb interaction effects in graphene bilayers: electron–hole pairing and plasmaron formation

Van-Nham Phan[1,2] **and Holger Fehske**[1,3]

[1] Institut für Physik, Ernst-Moritz-Arndt-Universität Greifswald, 17487 Greifswald, Germany
[2] Institute of Physics, Vietnamese Academy of Science and Technology, PO Box 429, 10000 Hanoi, Vietnam
E-mail: fehske@physik.uni-greifswald.de

New Journal of Physics **14** (2012) 075007 (11pp)
Received 19 January 2012
Published 3 July 2012
Online at http://www.njp.org/
doi:10.1088/1367-2630/14/7/075007

Abstract. We report a theoretical study of the many-body effects of electron–electron interaction on the ground-state and spectral properties of double-layer graphene. Using a projector-based renormalization method we show that if a finite-voltage difference is applied between the graphene layers, electron–hole pairs can be formed and—at very low temperatures—an excitonic instability might emerge in a double-layer graphene structure. The single-particle spectral function near the Fermi surface exhibits a prominent quasiparticle peak, different from neutral (undoped) graphene bilayers. Away from the Fermi surface, we find that the charge carriers strongly interact with plasmons, thereby giving rise to a broad plasmaron peak in the angle-resolved photoemission spectrum.

Contents

[3] Author to whom any correspondence should be addressed.

1. Motivation

Graphene-based structures are most likely the building blocks of future nanoelectronic devices. The reasons for this are manifold, but one may highlight that many of the exceptional properties of this new class of low-dimensional materials, which arise from the special form of the energy spectrum near the so-called Dirac nodal points and the related non-trivial topological structure of the wave function, can be easily modified by the application of external electric and magnetic fields, as well as by confining the sample geometry, by chemical doping or by edge functionalization and substrate manipulation; for recent reviews see [1–3].

Single-layer graphene (SLG) [4, 5], a truly two-dimensional (2D) crystal with remarkable mechanical properties, can be considered to be a gapless semiconductor with zero density of states at the Fermi level and a linear energy dispersion close to the (inequivalent) corners of the Brillouin zone (K, K′ Dirac points). Thus the low-energy electrons are massless, chiral Dirac fermions. As a consequence, any backscattering is suppressed and the charge carriers are almost insensitive to disorder and electron–electron interactions. Bilayer graphene (BLG) [6, 7], consisting of two AB-stacked, chemically bound graphene monolayers, is also a zero-gap semiconductor, if unbiased, but with a parabolic band dispersion. That is, in this material the low-energy electrons acquire a finite quasiparticle mass. Interestingly, there exists another physical realization of a graphene-based double-layer structure that can be fabricated: in this system—usually referred to as a graphene bilayer or double-layer graphene (DLG)—the two graphene sheets are separated by a dielectric so that the tunneling between the layers can be neglected [8–11].

In BLG and DLG, the charge carrier concentration can be controlled by the simple application of a gate voltage [7, 12]. This electric field effect is fundamental for potential technological applications. For BLG even the band structure might be manipulated by an electric field, so that a gap between the valence and conduction bands varies between zero and mid-infrared energies [13].

BLG, besides being at present the only known semiconductor with a tunable band gap, is intriguing also from a many-particle interaction physics perspective. While in SLG the interaction parameter is the fine-structure constant and Coulomb interaction effects are typically small, in BLG the interaction strength is alterable by changing the carrier density [14]. For DLG, the ability to modify the carrier polaribility of an individual layer even implies that the interlayer Coulomb interaction can be converted from repulsive to attractive [9]. Since a gate bias across the two-layered graphene leads to a charge imbalance in the layers, an attractive Coulomb interaction between the excess electrons and holes on opposite layers raises the possibility of formation of electron–hole bound states (excitons) [15]. Excitonic effects have been reported in the optical response of doped SLG [16] and BLG [17] as well. Most notably the BLG and DLG systems seem to be a promising candidate for electron–hole pair condensation [8, 9, 18–20]. In the weak coupling regime, exciton condensation is triggered by a Cooper-type instability of systems with occupied conduction-band states and empty valence-band states inside identical Fermi surfaces [18, 19, 21]. The particle–hole symmetry of the Dirac equation obviously ensures a perfect nesting between the electron Fermi surface and its hole counterpart in the n- and p-type layers of a biased DLG system [18]. A condensate of spatially separated electron–hole pairs might then occur when the interlayer tunneling is negligible, but the corresponding Coulomb interaction is not [8, 9]. Such bilayer exciton condensates typify as counterflow superfluids [22].

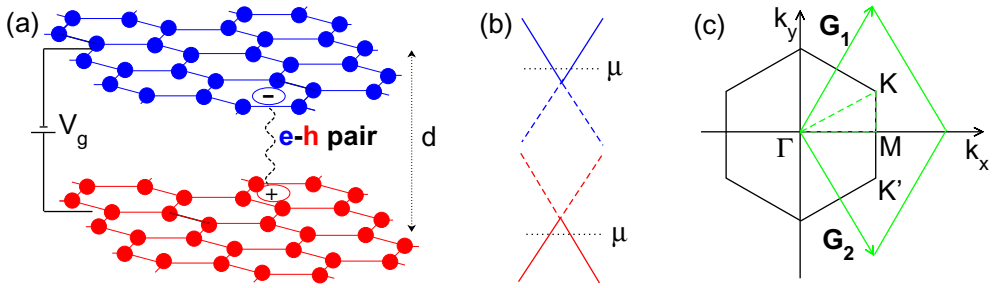

Figure 1. (a) Schematic diagram of a graphene bilayer system with electron and hole carriers induced by external gates forming excitonic bound states due to their Coulomb attraction. (b) The positions of the chemical potential in the two graphene layers are adjusted by the voltage V_g. (c) Brillouin zone of the graphene honeycomb lattice (black lines) and equivalent Brillouin zone (solid green lines) spanned by the inverse lattice vectors $\mathbf{G}_1$ and $\mathbf{G}_2$. Dirac cones are located at the K and K′ points.

In characterizing many-particle aspects of SLG, BLG and DLG, and in particular, the electron–electron, electron–hole and electron–plasmon interaction effects, the single-particle spectral function $A(k, \omega)$ gives detailed information. Angle-resolved photoemission spectroscopy (ARPES) is a powerful probe of $A(k, \omega)$ in (quasi-) 2D single-, bi- and few-layer graphene because it achieves frequency and momentum resolution and thereby directly addresses the quasiparticle energy band properties [7, 23, 24]. So far the spectral function of SLG and BLG has been calculated within the simple G_0W and random-phase approximation [14, 25–28], with a focus on dynamic screening, Kohn anomaly, Friedel oscillations and plasmons.

In this work, we employ the projector-based renormalization method (PRM) to determine the ground-state and spectral properties of an effective graphene bilayer model describing the interaction and possibly pairing of electrons from the top bilayer with holes from the bottom layer (see figure 1(a)). The topics of our main interest here are the effects of the Coulomb interaction on the formation of excitonic bound states and, for the doped system, the coupling between the charge carriers and plasmons leading to composite 'plasmaron' quasiparticles. We show that graphene-based bilayers might allow for electron–hole pair condensation and exhibit, in their ARPES spectra, pronounced plasmaron signatures away from the Dirac point.

2. Theoretical approach

We consider two graphene sheets separated by a dielectric thickness d, and assume a hexagonal stacking in which each sublattice in one layer is on top of the corresponding sublattice in the other layer [9]. Let now $V_g = eE_{ext}d$ be a gate-induced potential difference between the two layers. Then the external electric field E_{ext} outside the DLG system can be used to tune the chemical potential $\mu = V_g/2$ [18]: for a neutral graphene DLG system the Fermi level lies symmetrically in the conduction band of the upper (n-type) layer and in the valence band of the lower (p-type) layer (see figure 1(b)). Within an effective two-band description, the filled valence and empty conduction bands of the n- respectively p-type layers can be neglected

(dashed lines in panel (b)), and the Hamiltonian of the graphene bilayer, in the absence of the Coulomb interaction, is

$$\mathcal{H}_0 = g_s \sum_{\mathbf{k}} \varepsilon^+_{\mathbf{k}} a^\dagger_{\mathbf{k}} a_{\mathbf{k}} + g_s \sum_{\mathbf{k}} \varepsilon^-_{\mathbf{k}} b^\dagger_{\mathbf{k}} b_{\mathbf{k}}. \tag{1}$$

Here $a^\dagger_{\mathbf{k}}$ and $b^\dagger_{\mathbf{k}}$ are the creation operators of electron and hole quasiparticles with in-plane momentum $\mathbf{k}$ and band dispersions

$$\varepsilon^\pm_{\mathbf{k}} = \pm\gamma_0 \left[1 + 4\cos^2\frac{k_y}{2} + 4\cos\frac{k_y}{2}\cos\frac{\sqrt{3}}{2}k_x \right]^{1/2} \mp \mu, \tag{2}$$

which for momenta close to the Dirac points become the linear energy–momentum relations sketched by the blue and red straight lines in figure 1(b), respectively. In equations (1) and (2), $g_s = 2$ allows for the spin degeneracy and γ_0 denotes the nearest-neighbor transfer amplitude ($\gamma_0 \simeq 2.8\,\mathrm{eV}$ [1]).

In order to describe exciton formation, we take into account the interlayer coupling between electrons and holes,

$$\mathcal{H}_{\mathrm{e-h}} = \frac{g_s}{N} \sum_{\mathbf{k}_1\mathbf{k}_2,\mathbf{q}\neq 0} U_{\mathbf{k}_1\mathbf{k}_2\mathbf{q}}\, a^\dagger_{\mathbf{k}_1+\mathbf{q}} a_{\mathbf{k}_1} b^\dagger_{\mathbf{k}_2-\mathbf{q}} b_{\mathbf{k}_2}, \tag{3}$$

where

$$U_{\mathbf{k}_1\mathbf{k}_2\mathbf{q}} = \kappa \frac{\mathrm{e}^{-d|\mathbf{q}|}}{|\mathbf{q}|} \cos\frac{\phi_1}{2}\cos\frac{\phi_2}{2} \quad \text{with } \kappa = g_s\frac{2\pi\mathrm{e}^2}{\epsilon}. \tag{4}$$

The Coulomb matrix element $U_{\mathbf{k}_1\mathbf{k}_2\mathbf{q}}$ contains, in addition to the dielectric constant ϵ characterizing the embedding medium, a graphene-specific factor $\propto \cos\frac{\phi_1}{2}\cos\frac{\phi_2}{2}$, with scattering angles $\phi_i = \theta_{\mathbf{k}_i} - \theta_{\mathbf{k}_i+\mathbf{q}}$ where $\theta_{\mathbf{k}_i} = \mathrm{atan}(k_y/k_x)$ [9]. At this point at least two remarks are in order. Firstly, we have omitted the intralayer Coulomb repulsion between electrons or holes that manifests itself simply by a screening of the interlayer Coulomb interaction. For BLG it has been shown that the dynamically screened interlayer electron–hole interaction is attractive [8]. Secondly, the effective Coulomb attraction is long-ranged and depends in an involved way on the transmitted momentum. This is a major difference compared to the momentum-independent short-ranged Coulomb attraction in the extended Falicov–Kimball model, recently studied in the context of exciton formation and condensation within the PRM approach [29, 30]. Excluding the $\mathbf{q} = 0$ component (comprising the jellium background), the Hartree contributions to the one-particle energies vanish.

To proceed, we rewrite the total Hamiltonian, $\mathcal{H} = \mathcal{H}_0 + \mathcal{H}_{\mathrm{e-p}}$, in a normal-ordered form

$$\mathcal{H} = \sum_{\mathbf{k}} [\varepsilon^+_{\mathbf{k}} a^\dagger_{\mathbf{k}} a_{\mathbf{k}} + \varepsilon^-_{\mathbf{k}} b^\dagger_{\mathbf{k}} b_{\mathbf{k}} + (\Delta_{\mathbf{k}} b^\dagger_{\mathbf{k}} a_{\mathbf{k}} + \mathrm{h.c.})] + \frac{1}{N} \sum_{\mathbf{k}_1\mathbf{k}_2,\mathbf{q}\neq 0} U_{\mathbf{k}_1\mathbf{k}_2\mathbf{q}} : a^\dagger_{\mathbf{k}_1+\mathbf{q}} a_{\mathbf{k}_1} b^\dagger_{\mathbf{k}_2-\mathbf{q}} b_{\mathbf{k}_2} : \tag{5}$$

and look for a non-vanishing excitonic expectation value

$$\Delta_{\mathbf{k}} = -\frac{\kappa}{N} \sum_{\mathbf{q}} \frac{\mathrm{e}^{-d|\mathbf{q}|}}{|\mathbf{q}|} \frac{(1+\cos\phi)}{2} \langle a^\dagger_{\mathbf{k}+\mathbf{q}} b_{\mathbf{k}+\mathbf{q}} \rangle, \tag{6}$$

indicating a spontaneous symmetry breaking due to the pairing of electrons and holes. $\mathcal{H}$ is given in units of g_s, and $\phi = \theta_{\mathbf{k}+\mathbf{q}} - \theta_{\mathbf{k}}$.

Now the single-particle spectral function, e.g. for the conduction band electrons,

$$A^a(\mathbf{k},\omega) = -\frac{1}{\pi}\mathrm{Im}\, G^a(\mathbf{k},\omega), \tag{7}$$

with $G^a(\mathbf{k},\omega) = \langle\langle a_{\mathbf{k}}; a_{\mathbf{k}}^\dagger\rangle\rangle_{\mathcal{H}}$ being the Fourier transform of the retarded Green function ($\omega \to \omega + \mathrm{i}0^+$), can be computed by the PRM in close analogy to the calculation performed for the extended Falicov–Kimball model [29]. We have

$$G^a(\mathbf{k},\omega) = \langle\langle \tilde{a}_{\mathbf{k}}; \tilde{a}_{\mathbf{k}}^\dagger\rangle\rangle_{\tilde{\mathcal{H}}}, \tag{8}$$

where $\tilde{\mathcal{H}}$ is a renormalized Hamiltonian with all transition energies due to the interaction part of the Hamiltonian (5) successively integrated out. After this renormalization procedure becomes complete, $\tilde{\mathcal{H}}$ embodies a non-interacting Hamiltonian, but with a renormalized band structure, and therefore can be easily diagonalized by a Bogoliubov transformation to yield

$$\tilde{\mathcal{H}} = \sum_{\mathbf{k}} (E_{\mathbf{k}}^a \hat{a}_{\mathbf{k}}^\dagger \hat{a}_{\mathbf{k}} + E_{\mathbf{k}}^b \hat{b}_{\mathbf{k}}^\dagger \hat{b}_{\mathbf{k}}), \tag{9}$$

where

$$E_{\mathbf{k}}^{a/b} = \mp \frac{\mathrm{sgn}(\tilde{\varepsilon}_{\mathbf{k}}^- - \tilde{\varepsilon}_{\mathbf{k}}^+)}{2} W_{\mathbf{k}} + \frac{\tilde{\varepsilon}_{\mathbf{k}}^+ + \tilde{\varepsilon}_{\mathbf{k}}^-}{2} \quad \text{with } W_{\mathbf{k}} = [(\tilde{\varepsilon}_{\mathbf{k}}^+ - \tilde{\varepsilon}_{\mathbf{k}}^-)^2 + 4|\tilde{\Delta}_{\mathbf{k}}|^2]^{1/2}. \tag{10}$$

The new fermionic operators satisfy $\hat{a}_{\mathbf{k}} = u_{\mathbf{k}} a_{\mathbf{k}} + v_{\mathbf{k}} b_{\mathbf{k}}$ and $\hat{b}_{\mathbf{k}} = v_{\mathbf{k}} a_{\mathbf{k}} - u_{\mathbf{k}} b_{\mathbf{k}}$, with $u_{\mathbf{k}}^2 + v_{\mathbf{k}}^2 = 1$, $v_{\mathbf{k}}^2 = [1 - \mathrm{sgn}(\tilde{\varepsilon}_{\mathbf{k}}^- - \tilde{\varepsilon}_{\mathbf{k}}^+)(\tilde{\varepsilon}_{\mathbf{k}}^- - \tilde{\varepsilon}_{\mathbf{k}}^+)/W_{\mathbf{k}}]$. Replacing the renormalized quasiparticle operators $\tilde{a}_{\mathbf{k}}^\dagger = \tilde{x}_{\mathbf{k}} a_{\mathbf{k}}^\dagger + \frac{1}{N}\sum_{\mathbf{pq}} \tilde{y}_{\mathbf{kpq}} a_{\mathbf{k+q}}^\dagger : b_{\mathbf{p-q}}^\dagger b_{\mathbf{p}} :$ in equation (8), the spectral function is given to leading order in $\tilde{\Delta}$ by

$$A^a(\mathbf{k},\omega) = |\tilde{x}_{\mathbf{k}}|^2 \left[u_{\mathbf{k}}^2 \delta(\omega - E_{\mathbf{k}}^a) + v_{\mathbf{k}}^2 \delta(\omega - E_{\mathbf{k}}^b)\right] + \frac{1}{N^2}\sum_{\mathbf{pq}} |\tilde{y}_{\mathbf{kpq}}|^2$$
$$\times \delta\left(\omega - (E_{\mathbf{k+q}}^a - E_{\mathbf{p}}^b + E_{\mathbf{p-q}}^b)\right) [\langle \hat{n}_{\mathbf{k+q}}^a\rangle (\langle \hat{n}_{\mathbf{p-q}}^b\rangle - \langle \hat{n}_{\mathbf{p}}^b\rangle) + \langle \hat{n}_{\mathbf{p}}^b\rangle (1 - \langle \hat{n}_{\mathbf{p-q}}^b\rangle)]. \tag{11}$$

Note that the expectation values

$$\langle \hat{n}_{\mathbf{k}}^a\rangle = u_{\mathbf{k}}^2 f(E_{\mathbf{k}}^a) + v_{\mathbf{k}}^2 f(E_{\mathbf{k}}^b) \quad \text{and} \quad \langle \hat{n}_{\mathbf{k}}^b\rangle = v_{\mathbf{k}}^2 f(E_{\mathbf{k}}^a) + u_{\mathbf{k}}^2 f(E_{\mathbf{k}}^b) \tag{12}$$

have to be calculated with the fully renormalized Hamiltonian $\tilde{\mathcal{H}}$ as well, where $f(E_{\mathbf{k}}^{a,b})$ are Fermi functions. The spectral function for the valence-band holes, $A^b(\mathbf{k},\omega)$, is obtained in the exact same manner.

3. Results and discussion

The PRM approach outlined in the previous section must be numerically evaluated of course. In doing so, we work in the reciprocal space bounded by the green lines in figure 1(c), on a discrete set of $N = 64 \times 64$ points. Convergence of the whole renormalization scheme is assumed to be achieved if all quantities are determined with a relative error less than 10^{-5}. Thereafter the spectral functions are calculated using a Gaussian broadening in energy space of width 0.06. In what follows, we choose $\gamma_0 = 1$ as the unit of the energy, and measure all energies relative to the Dirac-point chemical potential of the balanced graphene bilayer. Furthermore, we fix the interlayer Coulomb coupling constant $\kappa = 7$; such a value can be realized with, e.g., the commonly used SiO_2 substrate/dielectric ($\epsilon \simeq 4$) [8].

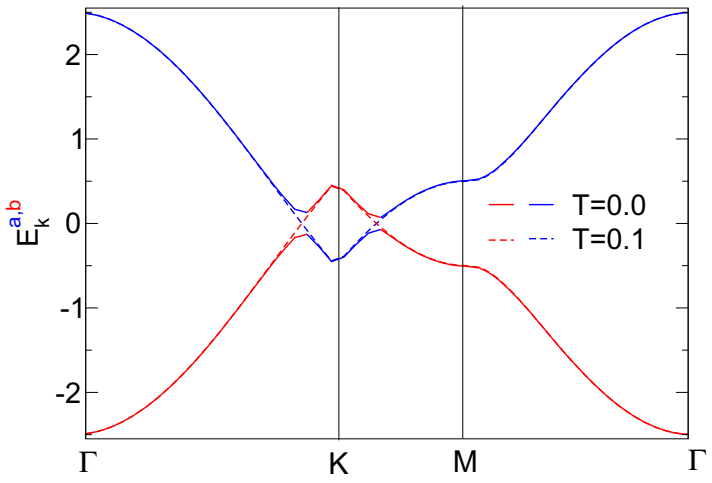

Figure 2. Renormalized band dispersions, $E^{a,b}_{\mathbf{k}}$, along the high-symmetry directions of the Brillouin zone of graphene, indicated in figure 1 by the dashed green lines. Results are given for an external field $E_{\rm ext} = 1$ at zero temperature (solid lines) and at $T = 0.1 > T_{\rm SF}$ (dashed lines).

Figure 2 shows how the band structure of such an interacting DLG system changes if the electric field $E_{\rm ext} = 1$ is applied. Apparently a pronounced excitonic gap appears at zero (low) temperatures[4]. The gap originates from electron–hole pair (exciton) condensation, driven by the attractive Coulomb interaction over the full bandwidth. In the result of this excitonic instability a macroscopically coherent quantum state emerges which, since electrons and holes are spatially separated in a graphene bilayer, differs in nature from the excitonic insulator phase in bulk 2D and 3D systems [30–38]. As can be seen from figure 2, the renormalized quasiparticle bands $E^{a,b}_{\mathbf{k}}$ possess a nearly perfect particle–hole symmetry. The gap disappears at higher temperatures when interlayer quantum coherence is destroyed by thermal fluctuations. For a strictly 2D system, of course, the critical temperature for exciton condensation would be zero, but the superfluid properties should survive for temperatures smaller than the Kosterlitz–Thouless transition temperature [9, 18]. Therefore, for the DLG system, our finite-temperature results will be valid for $T \leqslant T_{\rm KT}$ at least.

The zero- (low-) temperature exciton condensate is characterized by a non-vanishing expectation value $\delta_{\mathbf{k}} = \langle a^{\dagger}_{\mathbf{k}} b_{\mathbf{k}} \rangle$. Since the interlayer Coulomb interaction between electrons and holes is attractive for all momenta and we exclusively consider a uniform exciton condensate in DLG, $\delta = (1/N) \sum_{\mathbf{k}} \langle a^{\dagger}_{\mathbf{k}} b_{\mathbf{k}} \rangle$ can be taken as an adequate order parameter for the electron–hole pairing. This quantity is plotted in figure 3(a) against the magnitude of the electric field at zero temperature (red squares). It shows that above the threshold value $E_{\rm ext} \simeq 0.4$ the excitonic condensate becomes more robust as more charge carriers (electrons and holes) are induced into the layers by increasing the bias between them. Obviously, a larger valence and conduction band overlap amplifies the Cooper-like excitonic instability in the perfectly nested DLG system. Fixing $E_{\rm ext} = 1$, the order parameter is suppressed as the temperature increases (black circles), and vanishes when the electron–hole coherence is completely lost in the high-temperature phase. As it usually happens, the critical temperature itself is overestimated by theoretical approaches

[4] Note that the natural stacking in graphite is the Bernal stacking, which merely leads to an insignificantly smaller excitonic gap however; see figure 2 in [9].

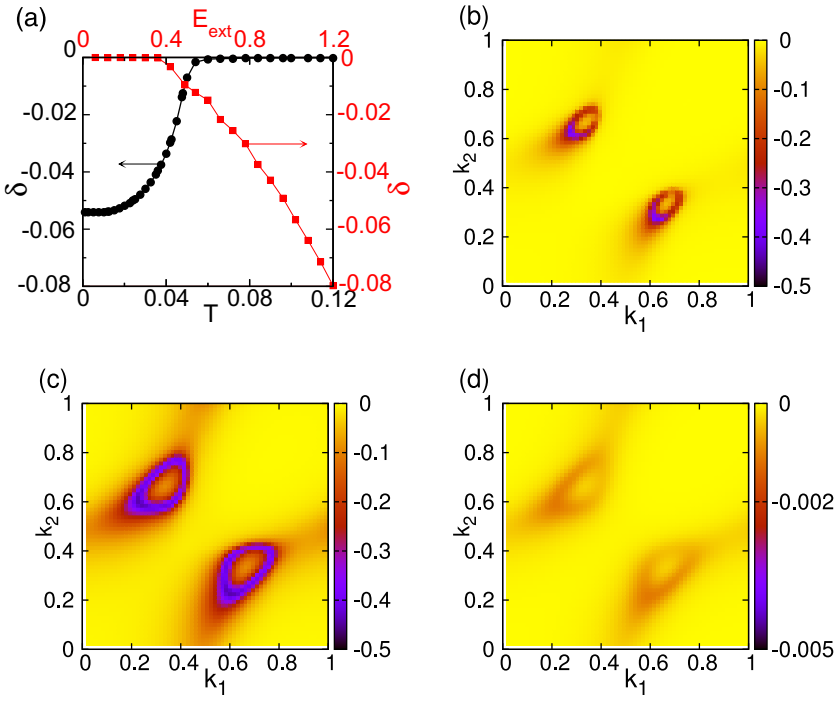

Figure 3. (a) Order parameter $\delta = (1/N)\sum_{\mathbf{k}}\langle a^{\dagger}_{\mathbf{k}} b_{\mathbf{k}}\rangle$ as a function of temperature T for an external electric field $E_{\rm ext} = 1$ (black circles) respectively as a function of $E_{\rm ext}$ at $T = 0$ (red squares). The other panels show the magnitude of the expectation value, $\delta_{\mathbf{k}} = \langle a^{\dagger}_{\mathbf{k}} b_{\mathbf{k}}\rangle$ with $\mathbf{k} = k_1\mathbf{G}_1 + k_2\mathbf{G}_2$, in reciprocal space by an intensity plot for $E_{\rm ext} = 0.6$, $T = 0$ (panel (b)), $E_{\rm ext} = 1$, $T = 0$ (panel (c)), and $E_{\rm ext} = 1$, $T = 0.1$ (panel (d); note the different intensity-color codings).

that comprise the electronic correlations and thermal fluctuations in an approximative way ($T_{\rm c} \sim 0.1$ eV for $E_{\rm ext} = 1$, see figure 3(a)). We note, however, that $T_{\rm c}$ is expected to be much larger than those of typical superconductors because exciton condensation is driven by the Coulomb interactions over the full bandwidth [18]. Panels (b)–(d) yield detailed information on the variation of the order parameter function $\delta_{\mathbf{k}}$ in the DLG Brillouin zone (here the diagonal belongs to the $\overline{\Gamma\mathrm{M}}$ direction). Raising the external electric field at zero temperature, exciton formation and condensation can set in if the conduction band of the upper layer enters the valence band of the lower layer. This takes place first at the Dirac points. If the electric field is enhanced further, electron and hole bands strongly hybridize along a crater-rim-shaped contour around K, K′, thereby establishing electron–hole coherence in this region (see panels (b) and (c)). Above a critical temperature $T > T_{\rm SF}$ this signature is washed out and $\delta_{\mathbf{k}}$ becomes basically zero anywhere.

To gain further insight into the Coulomb interaction effects in DLG, we now analyze the PRM results obtained for the total wave vector- and frequency-resolved single-particle spectral function $A(\mathbf{k}, \omega) = A^a(\mathbf{k}, \omega) + A^b(\mathbf{k}, \omega)$. Depending on the energy ω, $A(\mathbf{k}, \omega)$ measures the probability of finding an electron (hole) with momentum $\mathbf{k}$ in the system and is directly accessible by photoemission (inverse photoemission) experiments. Thereby it gives valuable information about the quasiparticle properties, in particular with regard to the quasiparticle dynamics.

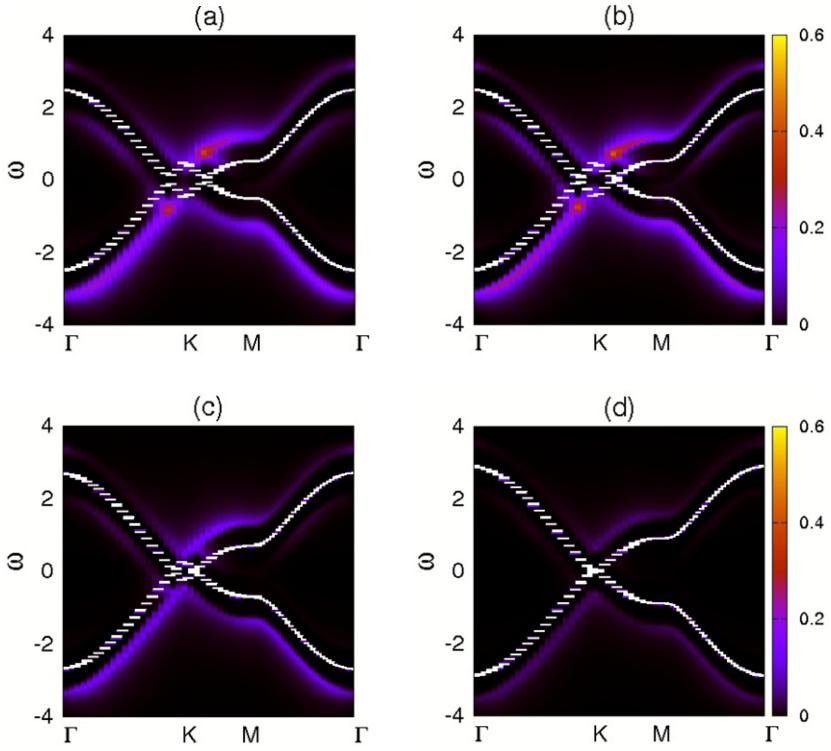

Figure 4. Intensity plots of the total wave vector-resolved single-particle spectral function $A(\mathbf{k}, \omega)$ for $T = 0$ and $E_{\text{ext}} = 1$ (panel (a)), respectively $T = 0.1$ and $E_{\text{ext}} = 1$ (b), 0.6 (c) and 0.2 (d).

A key question in this respect is whether the non-Fermi-liquid behavior observed for neutral undoped BLG/DLG at the Dirac point will survive in the presence of any doping. While Coulomb interactions self-evidently play no role for a pure zero-density Fermi system, i.e. will not affect this non-Fermi-liquid fix point, they become important at any finite carrier density (induced, e.g., by applying a gate voltage), or if spatially density fluctuations are present in real DLG samples. Using the random-phase and parabolic band approximations, it has been shown quite recently that BLG constitutes a Fermi liquid for doped cases, similar to the more standard 2D semiconductor-based electron gas [14]. If so, the Coulomb interaction should cause noticeable correlation effects.

Figure 4 gives the intensity of the single-particle spectral function, subject to ω along the high-symmetry directions of the Brillouin zone, for several characteristic situations. Panel (a) displays the behavior of $A(\mathbf{k}, \omega)$ when an exciton condensate is realized at $T = 0$. We find the location of the quasiparticle bands in accordance with the results of figure 2. These signatures have large spectral weight. Accordingly the effective-mass renormalization in DLG is expected to be rather weak, in contrast to the large mass renormalization in a normal 2D electron gas [14]. The single-particle excitation gap, located in the vicinity of the K point, disappears for $T = 0.1$ (panel (b)). That is, for $T > T_{\text{SF}}$ we have gapless excitations only. Panels (c) and (d) show how the overlap of the predominantly electron ($\omega > 0$) and hole ($\omega < 0$) quasiparticle bands shrinks as the electric field is reduced at a fixed temperature ($T = 0.1$).

In addition to the quasiparticle band signal discussed so far, we observe—especially in panels (a)–(c)—another signature that has less spectral weight, but is nevertheless well

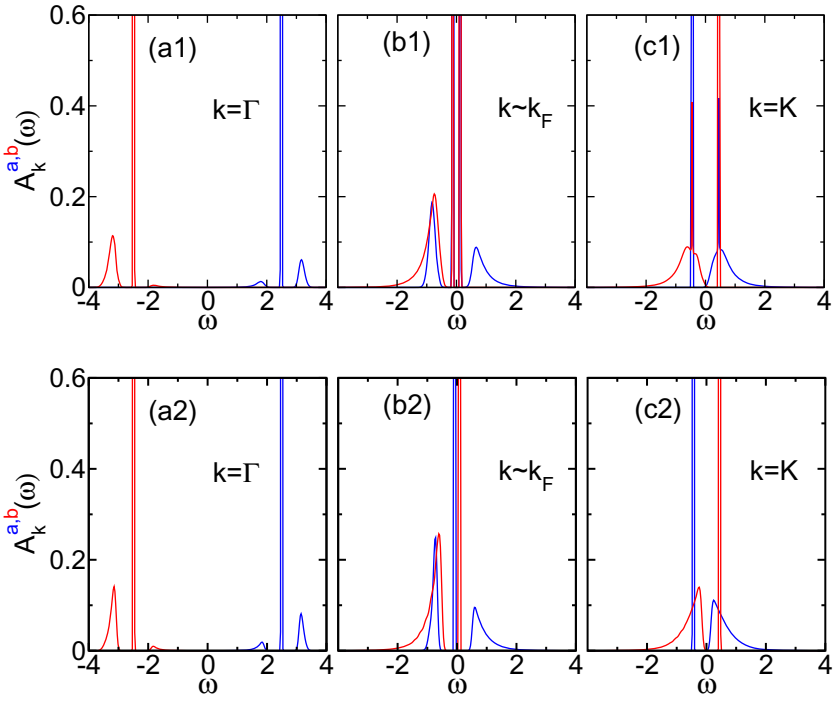

Figure 5. Single-particle spectral functions of conduction-band electrons $A^a(\mathbf{k}, \omega)$ (blue lines) and valence-band holes $A^b(\mathbf{k}, \omega)$ (red lines) plotted against ω for characteristic momenta $\mathbf{k} = \Gamma$ (left-hand (a) panels), $\mathbf{k} \sim \mathbf{k}_F$ (middle (b) panels), and $\mathbf{k} = K$ (right-hand (c) panels) at $T = 0.0$, $E_{ext} = 1.0$ (upper row 1) and $T = 0.1$, $E_{ext} = 1.0$ (lower row 2).

pronounced. It can be attributed to a plasmaron [39]. In an electron gas, the long-range Coulomb interaction manifests itself through plasmonic collective charge density oscillations. These plasmons can in turn interact with the charge carriers with the result that a new composite particle called a plasmaron is formed [39]. Plasmaron quasiparticles have been predicted to occur in SLG [25, 40, 41] and BLG [14], and were recently observed in the former system by ARPES [24]. Our, regarding the treatment of interaction and lattice structure effects, more involved PRM calculation corroborates this prediction for graphene bilayers. As can be seen from figure 4, satellite bands, arising from the dressing of the injected particle (electron or hole) by plasmon modes, appear away from the Fermi momentum. The plasmaron shows up at a greater (smaller) frequency than the quasiparticle because of the extra energy cost for the binding of the electron (hole) with the plasmon. The higher intensity of the plasmaron in the lower branch of the spectrum can be attributed to the fact that the plasmon oscillations are more pronounced in the p-type (few-hole) layer. The plasmaron signature weakens, of course, at very high doping level. Increasing the temperature, the plasmaron signal is slightly enhanced initially (since the electron–hole pairing is suppressed), but is finally smeared out when the temperature achieves the order of magnitude of the particle–plasmon binding energy. For small gate voltages (panel (d)), the plasmaron dispersion resembles that of SLG [40, 41], simply because the band overlap is small or even absent and the quasiparticles in the n- and p-type branches become uncorrelated.

Figure 5, finally, presents the frequency dependence of the partial electron and hole spectral functions at selected **k** points. It shows that the quasiparticles far away from the Fermi point are predominantly hole-like (red curves) or electron-like (blue curves) at both zero and finite temperature; see panels (a). This holds also for the corresponding plasmaron signatures. For $\mathbf{k} \simeq \mathbf{k}_{\mathrm{F}}$ (Fermi wave vector), the single-particle excitations are gapful (gapless) for $T = 0$ ($T > T_{\mathrm{SF}}$). Most notably, we observe a strong mixing of electron and hole bands, which also becomes apparent for the plasmarons. Moving to the K-point, this mixing is lost (see panels (c)), and the plasmaron bump appears well below (above) the corresponding electron (hole) quasiparticle peak.

4. Concluding remarks

Analyzing by means of a PRM the Coulomb interaction effects within a generic graphene bilayer model, we suppose that electron–hole pair formation and also condensation might appear in a DLG system at least at zero temperature if charge imbalance between the layers is induced by an external electric field. Thereby the condensation of the spatially separated but bounded electrons and holes turns out to be a robust phenomenon that will not require a precise alignment of the graphene sheets embedded in the dielectric [9, 18]. The excitonic instability is of Cooper (BCS) type, and manifests itself by an arising interlayer coherence between the electron and hole quasiparticles residing inside nearly perfectly nested Fermi surfaces. The condensed superfluid low-temperature state in DLG differs from the excitonic insulator state observed in (intermediate valent) rare-earth [33] or transition-metal systems [36]. The exciting BCS–BEC crossover upon an increase of the coupling strength [34, 37, 38], discussed for the latter materials as well as for standard semiconductor-based coupled quantum well structures, seems to be achievable in DLG in the presence of a perpendicular magnetic field only, when localized magnetoexcitons will form (see [8] and references therein). The pronounced quasiparticle peak in the single-particle spectra indicates that the electrons (holes) in doped DLG behave more like in a usual Fermi liquid. The ARPES spectra, in addition, feature a plasmaron peak, arising from the coupling of the charge carriers to collective density oscillations. Quite recently, the optical response of DLG for linearly polarized evanescent modes has been analyzed, showing exponential amplification for transverse polarization, which yields evidence for transverse plasmons, uniquely related to the chirality of the electronic carriers of graphene [11]. These effects might be of importance for the functionality of new plasmonic devices merging photonics and electronics [42, 43].

Acknowledgments

We thank K W Becker, F X Bronold, D Ihle, R Nandkishore and B Zenker for stimulating discussions. This work was supported by the DFG through SFB 652 and SPP 1459. V-N Phan was also financially supported by the National Foundation for Science and Technology Development (NAFOSTED) of Vietnam.

References

[1] Castro Neto A H, Guinea F, Peres N M R, Novoselov K S and Geim A K 2009 *Rev. Mod. Phys.* **81** 109
[2] Peres N M R 2010 *Rev. Mod. Phys.* **82** 2673
[3] Abergel D S L, Apalkov V, Berashevich J, Ziegler K and Chakraborty T 2010 *Adv. Phys.* **59** 261

[4] Novoselov K S, Geim A K, Morozov S V, Jiang D, Katsnelson M I, Grigorieva I V, Dubonos S V and Firsov A A 2005 *Nature* **438** 197
[5] Zhang Y, Tan Y W, Stormer H L and Kim P 2005 *Nature* **438** 201
[6] Novoselov K S, McCann E, Morozov S V, Fal'ko V I, Katsnelson M I, Zeitler U, Jiang D, Schedin F and Geim A K 2006 *Nature Phys.* **2** 177
[7] Ohta T, Bostwick A, Seyller T, Horn K and Rotenberg E 2006 *Science* **313** 951
[8] Lozovik Y E and Sokolik A A 2008 *JETP Lett.* **87** 55
[9] Zhang C H and Joglekar Y N 2008 *Phys. Rev.* B **77** 233405
[10] Ponomarenko L A *et al* 2011 *Nature Phys.* **7** 958
[11] Stauber T and Gómez-Santos G 2012 *Phys. Rev.* B **85** 075410
[12] Novoselov K S, Geim A K, Morozov S V, Jiang D, Zhang Y, Dubonos S V, Grigorieva I V and Firsov A A 2004 *Science* **306** 666
[13] Castro E V, Novoselov K S, Morozov S V, Peres N M R, dos Santos J M B L, Nilsson J, Guinea F, Geim A K and Neto A H C 2007 *Phys. Rev. Lett.* **99** 216802
[14] Sensarma R, Hwang E H and Das Sarma S 2011 *Phys. Rev.* B **84** 041408
[15] Dillenschneider R and Han J H 2008 *Phys. Rev.* B **78** 045401
[16] Yang L 2011 *Nano Lett.* **11** 3844
[17] Yang L, Deslippe J, Park C H, Cohen M L and Louie S G 2009 *Phys. Rev. Lett.* **103** 186802
[18] Min H, Bistritzer R, Su J J and MacDonald A H 2008 *Phys. Rev.* B **78** 121401
[19] Nandkishore R and Levitov K 2010 *Phys. Rev. Lett.* **104** 156803
[20] Hao N, Zhang P and Wang Y 2011 *Phys. Rev.* B **84** 155447
[21] Keldysh L V and Kozlov A N 1968 *Sov. Phys.—JETP* **27** 521
[22] Eisenstein J P and MacDonald A H 2004 *Nature* **432** 691
[23] Bostwick A, Ohta T, Seyller T, Horn K and Rotenberg E 2007 *Nature* **3** 36
[24] Bostwick A, Speck F, Seyller T, Horn K, Polini M, Asgari R, MacDonald A H and Rotenberg E 2010 *Science* **328** 999
[25] Polini M, Asgari R, Borghi G, Barlas Y, Pereg-Barnea T and MacDonald A H 2008 *Phys. Rev.* B **77** 081411
[26] Hwang E H and Das Sarma S 2008 *Phys. Rev. Lett.* **101** 156802
[27] Hwang E H and Das Sarma S 2008 *Phys. Rev.* B **77** 081412
[28] Sensarma R, Hwang E H and Das Sarma S 2010 *Phys. Rev.* B **82** 195428
[29] Phan V N, Becker K W and Fehske H 2010 *Phys. Rev.* B **81** 205117
[30] Phan V N, Fehske H and Becker K W 2011 *Europhys. Lett.* **95** 17006
[31] Keldysh L V and Kopaev H Y V 1965 *Sov. Phys.—Solid State* **6** 2219
[32] Halperin B I and Rice T M 1968 *Rev. Mod. Phys.* **40** 755
[33] Bucher B, Steiner P and Wachter P 1991 *Phys. Rev. Lett.* **67** 2717
[34] Bronold F X and Fehske H 2006 *Phys. Rev.* B **74** 165107
[35] Ihle D, Pfafferott M, Burovski E, Bronold F X and Fehske H 2008 *Phys. Rev.* B **78** 193103
[36] Monney C, Schwier E F, Garnier M G, Mariotti N, Didiot C, Cercellier H, Marcus J, Berger H, Titov A N, Beck H and Aebi P 2010 *New J. Phys.* **12** 125019
[37] Seki K, Eder R and Ohta Y 2011 *Phys. Rev.* B **84** 245106
[38] Zenker B, Ihle D, Bronold F X and Fehske H 2012 *Phys. Rev.* B **85** 121102R
[39] Lundquist B 1967 *Phys. Kondens. Mater.* **6** 193
[40] Hwang E H and Das Sarma S 2008 *Phys. Rev.* B **77** 115449
[41] LeBlanc J P F, Carbotte J P and Nicol E J 2011 *Phys. Rev.* B **84** 165448
[42] Rana F 2008 *IEEE Trans. Nanotechnol.* **7** 91
[43] Ryzhii M and Ryzhii V 2008 *Physics and Modeling of Tera- and Nano-Devices* (Singapore: World Scientific)